Research Paper

Ultrasonic Detection of Transversal Cracks in Rail Heads – Theoretical Approach

Tomasz KATZ[1)*], Sławomir MACKIEWICZ[1)], Zbigniew RANACHOWSKI[1)],
Zbigniew L. KOWALEWSKI[1)], Łukasz ANTOLIK[2)]

[1)] *Institute of Fundamental Technological Research*
Polish Academy of Sciences
Pawińskiego 5B, 02-106 Warsaw, Poland
*Corresponding Author e-mail: tkatz@ippt.pan.pl

[2)] *Railway Research Institute*
Chłopickiego 50, 04-275 Warsaw, Poland

In the paper the calculation of ultrasonic field generated by the transmitting transducer and the pulse-echo amplitude received after beam reflection at the defect in tested material is presented. The focus of the authors is directed on the specific transducer – defect configurations where the common methods of determination of ultrasonic beam trajectory fails. The developed analytical model is based on well-established principles of elastodynamic theory and forms the basis for computer program for simulation of ultrasonic examination of railway rails.

Key words: non-destructive testing; rolling contact fatigue damage; ultrasonic examination.

1. INTRODUCTION

The increase of the track loading due to traffic increment and introduction of high speed trains results in the occurrence of significant number of rolling contact fatigue (RCF) damages in exploited rails [1]. These faults may result in expansive cracks and finally cause rail breakage. The models of damage creation and growth in railway rails were described by CLAYTON *et al.* [2], BOLTON *et al.* [3], and FRANKLIN *et al.* [4]. Worldwide implemented rail line testing includes several non-destructive techniques, including: visual (VT), ultrasonic (UT), eddy current (ET) and magnetic (MT) [5]. In the European Union the standard EN 16729-3 [6] is observed in this respect.

One of the most difficult for detection rail defects are transversal cracks located in the rail head and oriented nearly vertically to the running surface of the rail head. Examples of rails broken due to the presence of aforementioned defects are shown in Fig. 1.
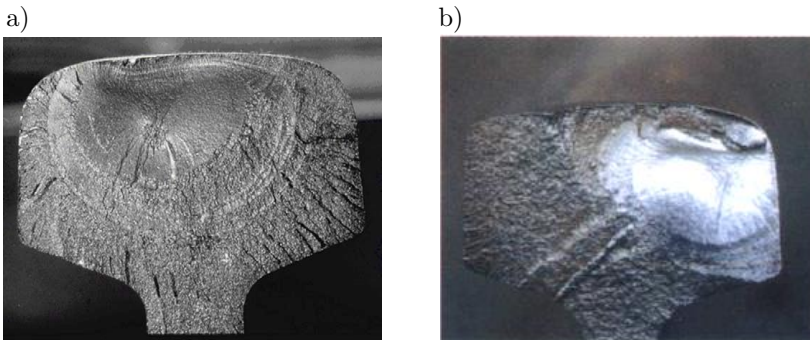
a) b)

Fig. 1. Examples of rail fractures caused by transversal fatigue cracks propagating
in nearly vertical direction.

According to EN 16729-1 for ultrasonic detection of transverse cracks in the
rail head the shear wave probes with refraction angle of 70° should be applied.
Conventionally, the testing system uses two T70° probes moved along the cen-
treline of the rail running surface and directed, respectively, in the forward and
backward direction. The aforementioned testing configuration (for one probe) is
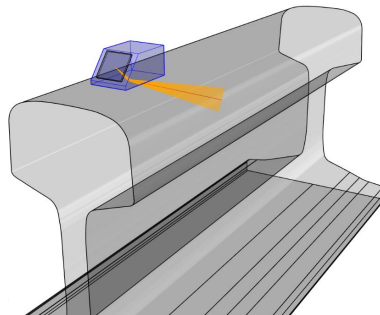shown in Fig. 2.

Fig. 2. The standard configuration of rail testing with T70° probe.
The image generated with use of Beam Tool 9 software package.

Unfortunately, this conventional testing method may be successful only in
detection of limited number of transversal cracks located in the central part
of the rail head. The cracks originating at the corner zones of the rail head
(as the one shown in Fig. 1b) are undetectable until they grow to the rail centre.
At that time they may already be big enough to cause a rail breakage resulting
in train derailment. Even if the transversal crack is located in the central part
of the rail head it is sometimes difficult to detect with standard T70°probes.
Such a problem occurs when the crack is nearly vertical and its surface is very
smooth (i.e. without kinks or folds). Relevant testing configuration is illustrated

in Fig. 3 together with a ray tracing picture generated with ultrasonic modelling software [8].
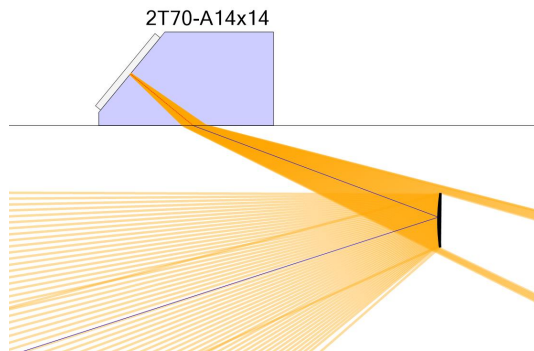

FIG. 3. Ray tracing modelling of ultrasonic beam interaction with vertical crack in rail head for a standard T70° probe.

Within the framework of the basic ray tracing propagation model such a crack geometry is completely undetectable with an angle beam probe, as all the rays incident on its surface are reflected in the lower direction, missing the testing probe. Fortunately, the ray tracing model is only the first approximation of the physical reality and, due to diffraction phenomena, some ultrasonic energy still returns to the testing probe and gives certain ultrasonic echo.

Considering the importance of this single problem for the reliability of inspection and safe operation of the railway lines, the authors undertook the efforts to increase the probability of detection of such defects by optimisation of ultrasonic testing methodology. The first stage of these efforts was to develop a theoretical model for adequate simulation of ultrasonic rail testing.

2. General description of modelling approach

As was already pointed out the basic ray tracing model [9], implemented in some commercial ultrasonic simulation software [8, 10] is not sufficient for adequate modelling of considered testing configuration due to ignoring diffraction in reflected beam. On the other hand the most accurate Finite Element Model (FEM) requires prohibitively high amount of computing power (and related costs) for typical modelling works requiring hundreds of simulations for different probes, defect positions and orientations [11, 12]. The FEM method is ineffective in simulation of ultrasonic testing problems due to the transient nature of the modelled phenomena (traveling pulses require hundreds of time domain iterations) and a short wavelength of ultrasonic waves compared to the typical sizes of tested objects. Because the FEM mesh step must be less than

c.a. 1/10 of ultrasonic wavelength, the sizes of meshes necessary for accurate simulations of 3D ultrasonic problems must be of the order of 10^9 or greater. So the best way for efficient, yet enough accurate modelling of ultrasonic testing problems seems to be semi-analytical model based on well-established theoretical foundations such as Rayleigh-Somerfield integral and elastodynamic Kirchhoff approximation [13]. The theoretical development of such simulation model is described in this paper.

The described model can be helpful in the efforts leading to design of the software aimed to simulate the interaction of ultrasonic beams and defects in rails. Such software has to be customized to testing of rails in the track where ultrasonic probes are moved over the top surface of the rail head. This is the only rail surface available for ultrasonic scanning in case of field inspections carried out nowadays with manual trolleys or inspection cars.

The simulation program should work within a framework of generic rail geometry whose exact dimensions can be adjusted to the specific rail type (UIC60, S49, etc.). It should enable simulation of ultrasonic beams generated by the broad class of ultrasonic probes, including standard angle and normal beam probes as well as dual element S and L-type probes. All basic parameters of the modelled ultrasonic probes, including frequency, transducer size and refraction angle should be freely adjusted as the input data. Except of a direct pulse-echo technique, the software should simulate examinations carried out with ultrasonic beam reflected off the bottom surface of the rail foot (corner effect) or the lower surfaces of the rail head. The ultrasonic beams may be directed along the rail axis or skewed to the rail side by defined angle.

Except the simulation and visualization of ultrasonic beams generated by the testing probes the program should calculate the amplitudes of ultrasonic echoes reflected from the standardized model defects. The standardized model defect adapted in the program is the disk shaped reflector (DSR) commonly used in ultrasonic testing as a reference reflector. The standard model defect can be implemented anywhere in the rail volume and have user defined size and orientation. It should be noted that such relatively simple idealization of real defects is quite adequate for considered examinations, as majority of real defects developing in railway rails during service are flat cracks of different size, position and orientation. The shapes of real rail defects can vary to a great extent and may considerably deviate from the circular shape of assumed model defect. Fortunately, this is not a major factor affecting the amplitude of received ultrasonic echoes as long as the position, orientation and surface area of defects are the same. The only characteristic of the real rail defects which cannot be adequately simulated by the implemented model defect is the surface roughness and unevenness. If the characteristic size of these features (e.q. R_a) is considerably smaller than the ultrasonic wavelength its influence can be neglected but if

it is comparable or greater than the ultrasonic wavelength the simulation results may considerably differ from measured echo amplitudes. This only emphasizes that simulation results must always be handled with great care and in depth knowledge of the nature and characteristics of the defects sought.

In practical testing of railway rails ultrasonic probes are mounted under the manual trolley or inspection car and moved along the rail with a certain speed. During such movement a multichannel ultrasonic system is simultaneously monitoring echo amplitudes from all testing channels and recording echo envelopes for all probes which receive signals exceeding the registration level. Based on the careful analysis of registered echo envelopes an ultrasonic expert evaluates the inspection results. To mimic this inspection reality the simulation software should allow for calculation of theoretical echo envelope for any implemented model defect.

As with any other theoretical modelling of the real word phenomena the simulation of ultrasonic testing is only a certain approximation of the reality. It can give more or less accurate predictions depending on accuracy and relevance of the theoretical model as well as on many side factors disturbing the real testing process which cannot be included in a theoretical model. In considered case these may be surface conditions of tested rails (deformed geometry, roughness, surface defects), quality of acoustic coupling, quality of ultrasonic probes and scanners, shadowing one defects by the another etc. The best evaluation of a theoretical model for a given application is achieved when a comparison of its predictions is done with well controlled experiments performed in conditions possibly close to the actual application conditions.

3. Calculation of ultrasonic field generated by the transmitting transducer

A theoretical model describing ultrasonic testing of a certain object must, first of all, allow for calculation of ultrasonic fields generated by different ultrasonic probes attached to its surface. This functionality is essential for planning testing procedures in such a way that all potential defects will be illuminated by ultrasonic beam of appropriate intensity coming from at least one testing probe. This is the first, but not the only, condition for successful ultrasonic examination.

We will consider standard ultrasonic testing configuration commonly used in ultrasonic testing of railway, shown in Fig. 4. The angle beam probe is coupled, with a thin layer of coupling medium, to the flat surface of tested object. The piezoelectric transducer attached to the refracting wedge made of plastic material (PMM, polystyrene) vibrates in a thickness mode and generates longitudinal wave in the wedge material. In line with common practice in ultrasonic

modelling we assume piston like transducer vibrations with angular frequency ω and uniform particle velocity v_0 over the whole surface. The ultrasonic wave propagating in the wedge hits the boundary between wedge and tested material at an angle α (see Fig. 4). From simple geometry consideration one can see that this angle is just equal to the wedge angle. The wedge angle α is selected between the 1st and 2nd critical angle so, that in the tested material is generated only one refracted, shear type wave.
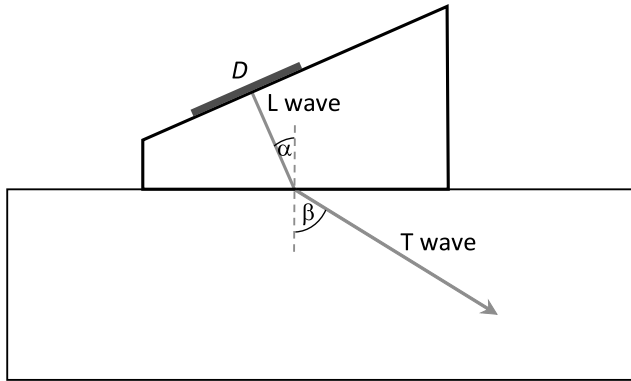

FIG. 4. Ultrasonic testing configuration with an angle beam probe coupled to the tested material.

The refraction angle of the shear wave β is related to the incidence angle of longitudinal wave α through the well-known Snell's law:

$$(3.1) \qquad \frac{\sin \alpha}{\sin \beta} = \frac{V_{L1}}{V_{T2}},$$

where V_{L1} is velocity of longitudinal (L-type) wave in wedge material, V_{T2} – velocity of transversal (T-type) wave in tested material.

Before we start calculation of ultrasonic field in the tested material we introduce certain simplifying assumption concerning wedge material. Because in the wedge we generate only longitudinal type of wave we will treat this material as an ideal fluid with the same mass density and velocity of longitudinal waves as the real wedge material. This way we neglect the wedge material shear stiffness which plays a marginal role in the analysed problem but would considerably complicate mathematical treatment. This assumption is also compatible with the fact that the probe wedge is coupled to the tested material with a thin layer of liquid which does not transmit shear stresses.

With this simplification we can use Rayleigh-Sommerfeld integral [13], known from fluid acoustics, for calculation of ultrasonic field in the wedge material.

The Rayleigh-Sommerfeld equation express the acoustic pressure p at point x in the fluid medium in terms of integral over the radiating transducer surface:

$$(3.2) \qquad p(\mathbf{x}) = \frac{-i\omega v_0 \rho_1}{2\pi} \int\limits_{S_t} \frac{e^{ikr}}{r} \, dS,$$

where ρ_1 is mass density of wedge material, ω is angular frequency of ultrasonic vibration, S_t is surface of the transmitting transducer, v_0 is normal particle velocity at the transducer surface, k is wavenumber of ultrasonic wave in the wedge, r is distance between the field point $\mathbf{x}$ and current integration point on the transducer surface.

The Rayleigh-Sommerfeld integral is a rigorous, mathematical formulation of the historical Huygens-Fresnel principle, which says that every point of vibrating surface (in our case the surface driven by transmitting transducer) is a source of secondary spherical wave and the interference of all these waves determines the form and amplitude of the primary wave at any subsequent time.

Using integral (3.2) we could easily calculate ultrasonic field in the wedge material, but this is not our final purpose. Actually, we want to calculate ultrasonic field in the tested material, i.e. after ultrasonic beam is refracted at the wedge-material boundary. In order to solve this more difficult problem we will use so called 'pencil model' first introduced by DESHAMPS [14] for calculations of electromagnetic beams generated by radars. This concept was later transferred to modelling of ultrasonic waves by CALMON at al. [15], RAILLON and LECOEUR-TAÏBI [16], and GENGEMBRE [17] and proved to be very effective in terms of calculation accuracy and computing efficiency. It is also quite intuitive and easy to understand for ultrasonic testing practitioners without in-depth knowledge of elastodynamic theory.

Consider certain fixed observation point P in tested material and arbitrary point source on the transducer surface (see Fig. 5). According to Fermat's prin-
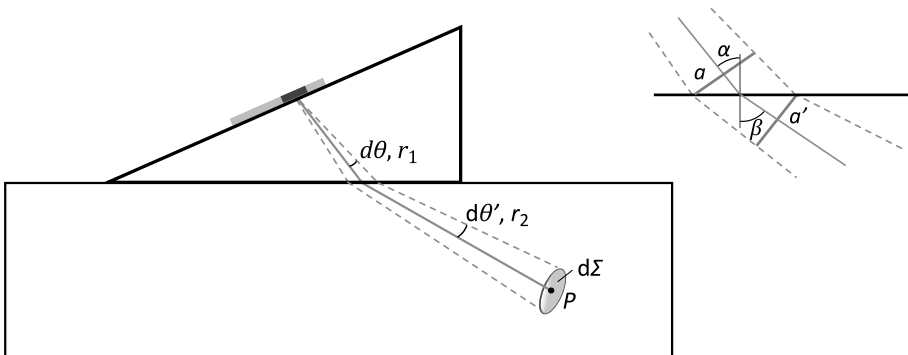

FIG. 5. Cone of rays (a pencil) located around the Fermat's path between an arbitrary point on the transducer surface and evaluation point P in the tested material.

ciple the acoustic energy generated by the source travels towards the observation point P along a particular trajectory, called the Fermat's path. The central ray of this path satisfies the Snell's law at the wedge-material border and the time of flight of ultrasonic wave along this path is the shortest of all possible paths. In more rigorous mathematical treatment this path is also called stationary phase path.

As was already noticed we will assume that the refracted wave is of the transversal type (T-type), as this is the most common configuration used in non-destructive testing. However, very similar reasoning could be performed for refracted longitudinal wave as well.

In order to evaluate the amplitude of an elementary wave going from the point source to the material point P, we will consider evolution of a wave cone starting at the source. Following the mentioned original works we will call this cone a pencil. The pencil is defined as a bunch of paraxial rays located infinitesimally close around the Fermat's central ray (see Fig. 5). Assuming that the total acoustic energy traveling in the pencil is constant, the change of the wave amplitude in the pencil may be determined by the evolution of its cross section area. Additionally, we have to take into consideration reduction of ultrasonic energy due to partial reflection at the wedge-material boundary. This is a fundamental assumption of the pencil's theory which holds well in all cases where the ultrasonic wavelength is much smaller than the curvature radii of the surfaces which refract or reflect ultrasonic beam.

Using the above assumptions of the pencil model we can derive an analogue of the Rayleigh-Sommerfeld integral valid in the tested material after refraction of the ultrasonic beam on the wedge-material border.

First, we will calculate the amplitude of the partial spherical wave generated by a point source on the transducer surface based on the pencil theory. According to Eq. (3.2) the ultrasonic energy emitted by a point source into the pencil cone with infinitesimal opening angle $d\theta$ is equal:

$$(3.3) \qquad dE_1 = \frac{p_1^2}{2z_1}\pi(d\theta)^2 = \frac{\omega^2 v_0^2 \rho_1^2}{8\pi^2 z_1}\pi(d\theta)^2,$$

where $z_1 = \rho_1 V_{L1}$ – acoustic impedance of the wedge material.

This energy is transferred within the pencil, without any losses, to the border between wedge and tested material. On the border plane the pencil is refracted according to the Snell's law (see Fig. 5) but part of its energy is reflected off, reducing the amount transmitted to the second medium.

The energy transmission coefficient at the border can be given by:

$$(3.4) \qquad T_{12}^E = \frac{v_2^2 z_2}{v_1^2 z_1}\frac{\cos\beta}{\cos\alpha} = (T_{12}^v)^2 \frac{z_2}{z_1}\frac{\cos\beta}{\cos\alpha},$$

where $z_2 = \rho_2 V_{T2}$ is acoustic impedance of the tested material, α is incidence angle of the pencil central ray, β is refraction angle of the pencil central ray, v_1 is particle velocity of the partial wave near the border in the first material, v_2 is particle velocity of the partial wave near the border in the second material, $T_{12}^v(\alpha)$ is transmission coefficient of particle velocity at the wedge-material border for a plane waves.

According to our previous assumptions the transmission coefficient $T_{12}^v(\alpha)$ should be the one relating longitudinal wave in the first fluid medium and transversal wave in the second solid medium. The mathematical formula for such transmission coefficient for plane waves can be found in many textbooks on ultrasonic wave theory, e.g. [13].

Combining Eqs (3.3) and (3.4) we can say that the acoustic energy traveling in the pencil after refraction is:

$$(3.5) \qquad \mathrm{d}E_2 = T_{12}^E \, \mathrm{d}E_1 = (T_{12}^v)^2 \frac{z_2}{z_1} \frac{\cos\beta}{\cos\alpha} \frac{\omega^2 v_0^2 \rho_1^2}{8\pi^2 z_1} \pi (\mathrm{d}\theta)^2.$$

Now, we should calculate the pencil cross section area $\mathrm{d}\Sigma$ at evaluation point P in the tested material using 3D geometry. The pencil starts at the point source on the transducer and initially forms a cone with a circular cross section and opening angle $\mathrm{d}\theta$. The pencil gradually increases its diameter, and at the wedge boundary reaches the value $a = 2r_1 \, \mathrm{d}\theta$, where r_1 is the path of the central ray in the wedge material.

At the wedge-material boundary, the central ray is refracted, together with all semi axial rays surrounding it. As a result the vertical cross section of the pencil changes (see Fig. 5) and can be expressed by the following formula:

$$(3.6) \qquad a' = \frac{\cos\beta}{\cos\alpha} a = \frac{\cos\beta}{\cos\alpha} 2r_1 \, \mathrm{d}\theta.$$

The pencil cross section in the plane perpendicular to the incidence plane (in the so called lateral plane) doesn't change and can be expressed as:

$$(3.7) \qquad a'' = a = 2r_1 \, \mathrm{d}\theta.$$

Geometrical analysis indicates that also divergence angles of the pencil change due to refraction. The new divergence angle in the incidence plane is given by:

$$(3.8) \qquad \mathrm{d}\theta' = \frac{V_{T2}}{V_{L1}} \frac{\cos\alpha}{\cos\beta} \, \mathrm{d}\theta$$

and in the lateral plane by:

$$(3.9) \qquad \mathrm{d}\theta'' = \frac{\sin}{\sin\alpha} \, \mathrm{d}\theta = \frac{V_{T2}}{V_{L1}} \, \mathrm{d}\theta.$$

We see, that after refraction the pencil is no longer a regular cone with circular cross-section but becomes more complex and characterized by elliptical cross-section. Nevertheless, knowing its dimensions at the border (a' and a'') and new divergence angles (θ' and θ'') we can easily calculate its dimensions (b' and b'') and cross-section area $d\Sigma$ at evaluation point P in the tested material:

$$(3.10) \qquad d\Sigma = \frac{\pi}{4}b'b'' = \frac{\pi}{4}\left(\frac{\cos\beta}{\cos\alpha}2r_1 + \frac{V_{T2}}{V_{L1}}\frac{\cos\alpha}{\cos\beta}2r_2\right)d\theta\left(2r_1 + \frac{V_{T2}}{V_{L1}}2r_2\right)d\theta.$$

After a few mathematical manipulations we obtain:

$$(3.11) \qquad d\Sigma = \left(\frac{\cos\beta}{\cos\alpha}r_1 + \frac{V_{T2}}{V_{L1}}\frac{\cos\alpha}{\cos\beta}r_2\right)\left(r_1 + \frac{V_{T2}}{V_{L1}}r_2\right)\pi(d\theta)^2.$$

As it was assumed in Eq. (3.2), $\mathbf{x}$ is a vector designating the position of the evaluation point P in the tested material. Now, combining Eqs (3.5) and (3.11) we obtain expression for the ultrasonic energy intensity $I(\mathbf{x})$ at the evaluation point P:

$$(3.12) \qquad I(\mathbf{x}) = \frac{dE_2}{d\Sigma} = \frac{\frac{\omega^2 v_0^2 \rho_1^2}{8\pi^2 z_1}(T_{12}^v)^2\frac{z_2}{z_1}\frac{\cos\beta}{\cos\alpha}}{\left(\frac{\cos\beta}{\cos\alpha}r_1 + \frac{V_{T2}}{V_{L1}}\frac{\cos\alpha}{\cos\beta}r_2\right)\left(r_1 + \frac{V_{T2}}{V_{L1}}r_2\right)}.$$

But, the energy intensity I of a plane or a quasi-plane ultrasonic wave is directly related to the amplitude of partial velocity of that wave by the standard formula:

$$(3.13) \qquad I = \frac{1}{2}z_2 v_2^2.$$

Making use of that formula we can obtain an expression for the amplitude of particle velocity of a partial wave at the point P with the coordinate vector $\mathbf{x}$:

$$(3.14) \quad |v_2(\mathbf{x})| = \sqrt{2I/z_2} = \frac{\omega v_0}{2\pi V_{L1}}T_{12}^v\sqrt{\frac{\frac{\cos\beta}{\cos\alpha}}{\left(\frac{\cos\beta}{\cos\alpha}r_1 + \frac{V_{T2}}{V_{L1}}\frac{\cos\alpha}{\cos\beta}r_2\right)\left(r_1 + \frac{V_{T2}}{V_{L1}}r_2\right)}}$$

$$= \frac{\omega v_0}{2\pi V_{L1}}T_{12}^v\frac{1}{\sqrt{\left(r_1 + \frac{V_{T2}}{V_{L1}}\frac{\cos^2\alpha}{\cos^2\beta}r_2\right)\left(r_1 + \frac{V_{T2}}{V_{L1}}r_2\right)}}.$$

The phase of the partial wave at the point P results from the passage of the pencil central ray through the section r_1 in the wedge material and section r_2 in the tested material and equals: $k_1 r_1 + k_2 r_2$. Additionally we add a factor $-i$ to ensure phase continuity with Eq. (3.2) at the wedge-material boundary. As a result

the final complex expression for the amplitude of the partial wave at the field point P takes the form:

$$(3.15) \qquad v_2(\mathbf{x}) = \frac{-i\omega v_0}{2\pi V_{\text{L1}}} \frac{T_{12}^v(\alpha)e^{i(k_1 r_1 + k_2 r_2)}}{\sqrt{\left(r_1 + \frac{V_{\text{T2}}}{V_{\text{L1}}}\frac{\cos^2\alpha}{\cos^2\beta}r_2\right)\left(r_1 + \frac{V_{\text{T2}}}{V_{\text{L1}}}r_2\right)}}.$$

In Eq. (3.15), we indicated that transmission coefficient T_{12}^v depends on the incidence angle α of the pencil central ray and thus it is different for each point source on the transducer surface.

Now, we can calculate the total ultrasonic field at the point P by summing up amplitudes of all partial waves coming from all point sources distributed over the transmitting transducer surface. The resulting integral over transducer surface S_t takes the form:

$$(3.16) \qquad v(\mathbf{x}) = \frac{-i\omega v_0}{2\pi V_{\text{L1}}} \int_{S_t} \frac{T_{12}^v(\alpha)e^{i(k_1 r_1 + k_2 r_2)}}{\left(r_1 + \frac{V_{\text{T2}}}{V_{\text{L1}}}\frac{\cos^2\alpha}{\cos^2\beta}r_2\right)^{1/2}\left(r_1 + \frac{V_{\text{T2}}}{V_{\text{L1}}}r_2\right)^{1/2}} \, dS,$$

where $v(\mathbf{x})$ is the complex partial velocity amplitude of ultrasonic wave generated by the whole transmitting transducer.

It should be noted that in Eq. (3.16) we sum up particle velocities of partial waves as simple scalars, without regarding its true vector nature. It is simplification typical for all scalar theories of diffraction. The scalar value describing the ultrasonic field amplitude is quite suitable and adequate for presentations of ultrasonic field distributions on 2D maps or cross-sections. But, for some other applications we need the full vector value of particle velocity which completely describes the ultrasonic field.

We can estimate the missing direction of particle vibrations in the far field of transmitting transducer in the following way. First of all, in the far field the generated wave can be approximated by a divergent beam of quasi-plane waves with virtual centre located at the centre of the transmitting transducer (see Fig. 6). So, the ray starting at the transducer centre and reaching the evaluation point P is perpendicular to the wave front at this point. Consequently, the directional versor of the wave at this point $\mathbf{e}_i$ is determined by the direction of this central ray and polarity versor $\mathbf{d}_{i\text{SH}}$ by the cross section of the plane perpendicular to $\mathbf{e}_i$ and the plane of incidence of the aforementioned ray on the wedge-material border.

Comparing Eq. (3.16) to the original form of Rayleigh-Sommerfeld integral (3.6) one may notice that we have changed the physical quantity which describes the ultrasonic field. The acoustic pressure $p(\mathbf{x})$ is not well defined for solid medium so we have changed it for the particle velocity $v(\mathbf{x})$ which is well defined

for both fluids and elastic solid media. Second difference compared to the formula (3.2) is replacement of a simple divergence factor $1/r$ with a more complex expression combining r_1 and r_2. It follows from the fact that partial waves in the second medium are no longer simple spherical waves, but form more complex wave fronts. The presence of the transmission coefficient T_{12}^v is rather obvious as the partial waves pass through the boundary of materials.

The last important consideration is connected with the fact that in ultrasonic modelling for non-destructive testing we actually do not need the absolute values of ultrasonic amplitudes but only its relative values and space distributions. In practice, we always compare received echoes with some reference echoes obtained from predefined artificial reflectors (FBH, SDH, BW). So, we can further simplify formula (3.16) by replacing all constant values before integral with 1 to obtain integral expression for normalised value of ultrasonic wave amplitude

$$(3.17) \qquad \overline{v}(\mathbf{x}) = \int\limits_{S_t} \frac{T_{12}^v(\alpha) e^{i(k_1 r_1 + k_2 r_2)}}{\left(r_1 + \frac{V_{\mathrm{T2}}}{V_{\mathrm{L1}}} \frac{\cos^2\alpha}{\cos^2\beta} r_2 \right)^{1/2} \left(r_1 + \frac{V_{\mathrm{T2}}}{V_{\mathrm{L1}}} r_2 \right)^{1/2}} \, \mathrm{d}S.$$

All factors included in integral (3.17) can be readily calculated if we can determine α, β, r_1, and r_2 for any combination of a source point on the transducer surface and evaluation point in the tested material (see Fig. 5). This problem is equivalent to determining the Fermat path between two given points. It can be easily solved using a numerical algorithm looking for minimum time of flight of ultrasonic wave between two such points.

4. Calculation of ultrasonic echo amplitude

Determination of ultrasonic field generated by the transmitting transducer is the first step in numerical simulation of ultrasonic inspection. Using this possibility we can check if the ultrasonic beam actually illuminates defects positioned in different parts of the tested object with sufficient amplitude. However looking at Fig. 3 we can immediately conclude that the proper illumination of defect with ultrasonic beam does not guarantee its detection. This heavily depends on defect orientation and size.

So, the next important step in modelling efforts is calculation of the height of ultrasonic echo received after reflection/scattering at the model defect. To solve this rather difficult task we will make use of the electromechanical reciprocity theorem [17, 18] which considerably simplifies the mathematical treatment. The reciprocity concept allows us to assume that the sensitivity field of the receiving transducer is the same as the actual ultrasonic field of the same transducer when working as a transmitter. This way, we can use the equations derived in the previous chapter to calculate the sensitivity fields of the receiving transducers.

The subject of detection are secondary sources generated on the defect surface by the incident ultrasonic wave.

The secondary point sources on the defect surface generate partial spherical waves the same way as point sources distributed over the transmitting transducer surface. The problem is, that the amplitudes and directions of their vibrations are not known a priori, as it was in the case of transmitting transducer. They must be calculated based on the amplitude and direction of the incident wave and its interaction with the defect surface.

In general solving this type of problem is very difficult but under some simplifying assumptions we can treat it using quite effective semi analytic approach. First of all, we define our model defect as a disc shape reflector (DSR) with an ideally flat and traction free surfaces. We will allow the model defect to have any diameter and orientation within the tested object. The general scheme of interaction of incident wave with our model defect is depicted in Fig. 6.
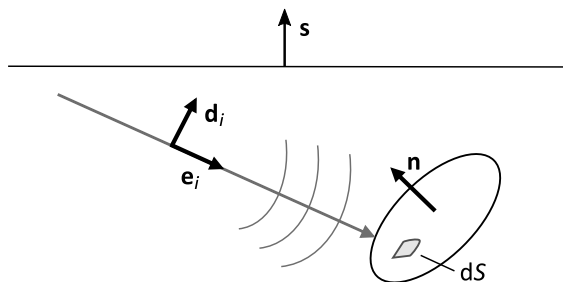

FIG. 6. Interaction of incident transversal ultrasonic wave with a model defect.

The transversal wave generated by the transmitting transducer hits the surface of the model defect of diameter D and normal versor $\mathbf{n}$. The wave striking certain small element $\mathrm{d}S$ on the defect surface can be characterised by its direction $\mathbf{e}_i$, polarisation $\mathbf{d}_i$ and amplitude of particle velocity v_i. The result of this wave interaction with the surface element depends on incidence angle, as well as, on the orientation of its polarisation versor $\mathbf{d}_i$ with respect to the plane of incidence on the defect surface. Generally, any incident shear wave can be decomposed into two standard polarities called SV (shear vertical) and SH (shear horizontal). These polarities are considered in relation to the reflecting surface, that is the surface of the model defect. The interaction of both types of waves with stress free plane is illustrated in Fig. 7.

To go further we must introduce very important assumption known as the elastodynamic Kirchhoff approximation [18]. It states that the ultrasonic wave hitting the defect surface at a certain point reflects from it in the same way as an ideal plane wave from the infinite plane, parallel to the defect surface at that interaction point. As the surface of our model defect is flat and its surfaces
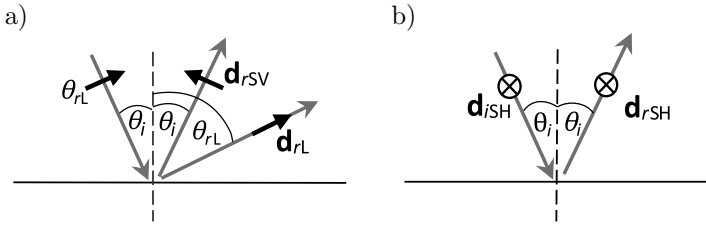
a)　　　　　　　　　　　　　　　　b)

FIG. 7. Interaction of SV and SH waves with a stress free plane.

are stress free, it seems a quite reasonable assumption. The only difference is that our defect is not infinite (has diameter D) and our ultrasonic beam is not a plane wave. So, we can expect that Kirchhoff approximation will work well, only if defect is located in the far field of transmitting transducer (where the incident ultrasonic wave becomes a semi plane wave) and its size is considerably greater than the ultrasonic wavelength. Those conditions are generally met in ultrasonic testing of railway rails but the actual degree of compliance can only be confirmed in experimental verification. By adopting Kirchhoff approximation we can use in our model the well-known canonical solutions obtained for plane waves.

First, we consider the case when incident wave is of SV type. For such a case there are generally two types of reflected waves, SV-type and L-type. The SV wave reflects at an angle equal to the incidence angle: $\theta_{r\mathrm{SV}} = \theta_i$. Its direction versor $e_{r\mathrm{SV}}$ and polarisation versor $d_{r\mathrm{SV}}$ can be calculated based on the knowledge of e_i and $d_{i\mathrm{SV}}$ for the incidence wave

$$(4.1) \qquad \mathbf{e}_{r\mathrm{SV}} = \mathbf{e}_i - 2(\mathbf{e}_i \cdot \mathbf{n})\mathbf{n},$$

$$(4.2) \qquad \mathbf{d}_{r\mathrm{SV}} = 2(\mathbf{d}_{i\mathrm{SV}} \cdot \mathbf{n})\mathbf{n} - \mathbf{d}_{i\mathrm{SV}}.$$

The L-type wave reflects at an angle $\theta_{r\mathrm{L}}$ resulting from the Snell's law and have polarization direction $\mathbf{d}_{r\mathrm{L}}$ parallel to the propagation direction $\mathbf{e}_{r\mathrm{L}}$. These versors can be calculated in the following way.

From the Snell's law it follows that the component of $\mathbf{e}_{r\mathrm{L}}$ parallel to the reflecting plane is equal:

$$(4.3) \qquad \mathbf{e}_{r\mathrm{L}}^{\parallel} = \frac{V_{\mathrm{L}2}}{V_{\mathrm{T}2}}\left[\mathbf{e}_i - (\mathbf{e}_i \cdot \mathbf{n})\mathbf{n}\right].$$

Consequently, the versor component perpendicular to the reflecting plane must be

$$(4.4) \qquad \mathbf{e}_{r\mathrm{L}}^{\perp} = \sqrt{1 - \left|\mathbf{e}_{r\mathrm{L}}^{\parallel}\right|^2}\,\mathbf{n}.$$

Finally, the full versor $\mathbf{e}_{rL}$ is given by

$$(4.5) \qquad \mathbf{e}_{rL} = \mathbf{e}_{rL}^{\parallel} + \mathbf{e}_{rL}^{\perp}.$$

The polarisation versor of longitudinal wave is parallel to its direction and given by:

$$(4.6) \qquad \mathbf{d}_{rL} = \mathbf{e}_{rL}.$$

To fully characterize reflected waves we need not only their directions and polarisations but also their amplitudes. Thanks to the Kirchhoff approximation they can be easily calculated using reflection coefficients $R^{(\mathrm{SV,SV})}$ and $R^{(\mathrm{L,SV})}$ for the plane waves. Using these coefficients we ultimately get the expression for the particles velocity on the defect surface caused by SV component of the incident wave:

$$(4.7) \qquad \mathbf{v}_{\mathrm{SV}}^{(1)} = v_{\mathrm{SV}}\left(\mathbf{d}_{i\mathrm{SV}} + R^{(\mathrm{SV,SV})}\mathbf{d}_{r\mathrm{SV}} + R^{(\mathrm{P,SV})}\mathbf{d}_{rL}\right).$$

Reflection coefficients $R^{(\mathrm{SV,SV})}$ and $R^{(\mathrm{L,SV})}$ depend on the incident angle θ_i of ultrasonic wave at the surface element $\mathrm{d}S$. Also the amplitude of SV component of incident wave v_{SV} changes over the defect surface.

Next, we consider the case when an incident wave is of SH type. For such a case there is only one reflected wave of SH-type (see Fig. 7b). The SH wave reflects at an angle equal to the incidence angle $\theta_{r\mathrm{SH}} = \theta_i$. Its direction and polarisation versors can be calculated based on the $\mathbf{e}_i$ and $\mathbf{d}_{i\mathrm{SH}}$ versors of the incidence wave:

$$(4.8) \qquad \mathbf{e}_{r\mathrm{SH}} = \mathbf{e}_i - 2(\mathbf{e}_i \cdot \mathbf{n})\mathbf{n},$$

$$(4.9) \qquad \mathbf{d}_{r\mathrm{SH}} = \mathbf{d}_{i\mathrm{SH}}.$$

In this case all the incident ultrasonic energy reflects as SH wave so the reflection coefficient $R^{(\mathrm{SH,SH})} = 1$. Using this we get an expression for the particles velocity of surface vibrations caused by SH component of the incident waves:

$$(4.10) \qquad \mathbf{v}_{\mathrm{SH}}^{(1)} = v_{\mathrm{SH}}\left(\mathbf{d}_{i\mathrm{SH}} + R^{(\mathrm{SH,SH})}\mathbf{d}_{r\mathrm{SH}}\right) = 2v_{\mathrm{SH}}\,\mathbf{d}_{i\mathrm{SH}}.$$

Having calculated particle velocity amplitudes for both components (SV and SH) of the incident wave we can calculate the total particles velocity of ultrasonic vibrations at the defect surface. It is equivalent to the amplitude of secondary point sources at infinitesimal surface elements $\mathrm{d}S$:

$$(4.11) \qquad \mathbf{v}^{(1)} = \mathbf{v}_{\mathrm{SV}}^{(1)} + \mathbf{v}_{\mathrm{SH}}^{(1)}.$$

Now we may recall the strict mathematical formulation of the reciprocity theorem applicable directly to our problem, developed by SCHMERR [13]:

$$(4.12) \qquad F_B = \frac{1}{v_0^{(2)}} \int\limits_{S_d} \left(\tau_{ji}^{(1)} v_i^{(2)} - \tau_{ji}^{(2)} v_i^{(1)} \right) n_j \, \mathrm{d}S,$$

where F_B is blocked force exerted on the receiving transducer by ultrasonic wave reflected from the defect, $v_i^{(1)}$ are components of particle velocity amplitude for solution (1), $v_i^{(2)}$ are components of particle velocity amplitude for solution (2), $\tau_{ji}^{(1)}$ are components of stress tensor for solution (1), $\tau_{ji}^{(2)}$ are components of stress tensor for solution (2), $v_0^{(2)}$ is amplitude of receiving transducer vibrations for solution (2), n_j are components of versor **n** normal to the model defect.

Fields marked with superscript (1) in the above equation refer to the solution of the problem we considered before, where the transmitting transducer generates ultrasonic field which interacts with model defect. Fields marked with superscript (2) refer to an auxiliary solution where the <u>receiving transducer</u> acts as a piston like source vibrating with velocity $v_0^{(2)}$ and generating in the tested material an ultrasonic field which <u>do not interact</u> with the model defects. This field can be interpreted as sensitivity field of the receiving transducer. We can calculate it in the same way as regular fields generated by transmitting transducers, using formula (3.17). The blocked force on the left side of Eq. (4.12) is the total force exerted on the face of receiving transducer by the ultrasonic wave reflected from the model defect, under assumption that this face is held rigidly fixed (is blocked). The amplitude of ultrasonic echo displayed by ultrasonic flaw detector connected to the receiving transducer is proportional to this blocked force value [19].

Considering that our model defect is crack like, we assume that it has stress free surfaces $\tau_{ji}^{(1)} = 0$ what simplifies Eq. (4.12) to the form:

$$(4.13) \qquad F_B = \frac{-1}{v_0^{(2)}} \int\limits_{S_d} \tau_{ji}^{(2)} v_i^{(1)} n_j \, \mathrm{d}S.$$

It should be noted that $\tau_{ji}^{(2)}$ <u>is not zero</u> on the defect surface as the solution (2) neglects the presence of the model defect in the tested material.

Now, we have to calculate stress components $\tau_{ji}^{(2)}$ of solution (2) based on ultrasonic field amplitude calculated from Eq. (3.17) and additional considerations concerning particle velocity direction. We start with a standard stress-strain relation for elastic solid:

$$(4.14) \qquad \tau_{ij}^{(2)} = C_{ijkl} e_{kl}^{(2)} = C_{ijkl} \frac{1}{2} \left(\frac{\partial u_k^{(2)}}{\partial x_l} + \frac{\partial u_l^{(2)}}{\partial k} \right) = C_{ijkl} \frac{\partial u_k^{(2)}}{\partial x_l},$$

where $u_k^{(2)}$ are components of displacement vector for solution (2), $e_{kl}^{(2)}$ are components of strain tensor for solution (2), C_{ijkl} are components of stiffness tensor for tested material.

Stiffness tensor C_{ijkl} for the isotropic solid can be given by [20]:

$$(4.15) \qquad C_{ijkl} = \lambda \delta_{ij} \delta_{kl} + \mu \left(\delta_{ik} \delta_{jl} + \delta_{il} \delta_{jk} \right),$$

where λ, μ is Lame constants for the tested material, δ_{kl} is delta Kronecker symbol.

Now, we need expressions for $u_k^{(2)}$ and its spatial derivatives:

$$(4.16) \qquad u_k^{(2)} = \frac{1}{-i\omega} v^{(2)} d_k^{(2)},$$

$$(4.17) \qquad \frac{\partial u_k^{(2)}}{\partial x_l} = \frac{ik_t}{-i\omega} v^{(2)} d_k^{(2)} e_l^{(2)} = \frac{-1}{V_{\mathrm{T}2}} v^{(2)} d_k^{(2)} e_l^{(2)},$$

where k_t is wavenumber for shear wave in tested material, $v^{(2)}$ is amplitude of ultrasonic particle velocity for solution (2), $d_k^{(2)}$ are components of the polarisation versor for solution (2), $e_l^{(2)}$ are components of the direction versor for solution (2).

The scalar amplitude $v^{(2)}$ of particle velocity can be calculated from modified Rayleigh-Sommerfeld integral (3.17) by replacing transmitting transducer with the receiving one. The directional versor $\mathbf{e}^{(2)}$ of the ray coming from the centre of the receiving transducer to the integration point on the defect surface can be calculated based on the position of the receiving probe on the tested object. The polarisation versor $\mathbf{d}^{(2)}$ is perpendicular to direction versor $\mathbf{e}^{(2)}$ and is lying in the plane of incidence of this central ray on the material surface. It can be determined from the equation:

$$(4.18) \qquad \mathbf{d}^{(2)} = \frac{\mathbf{e}^{(2)} \times \mathbf{s}}{\left| \mathbf{e}^{(2)} \times \mathbf{s} \right|} \times \mathbf{e}^{(2)},$$

where $\mathbf{s}$ is the versor normal to the tested material surface (see Fig. 6).

Substituting Eq. (4.17) to the integral (4.13) we obtain:

$$(4.19) \quad F_B = \frac{-1}{v_0^{(2)}} \int_{S_d} \tau_{ji}^{(2)} v_i^{(1)} n_j \, \mathrm{d}S$$

$$= \frac{-1}{v_0^{(2)}} \int_{S_d} [\lambda \delta_{ij} \delta_{kl} + \mu \left(\delta_{ik} \delta_{jl} + \delta_{il} \delta_{jk} \right)] \frac{-1}{V_{\mathrm{T}2}} v^{(2)} d_k^{(2)} e_l^{(2)} v_i^{(1)} n_j \, \mathrm{d}S.$$

This, rather complex expression can be considerably simplified using properties of delta Kronecker symbols present in the integrand.

$$(4.20) \quad F_B = \frac{1}{v_0^{(2)} V_{\text{T2}}} \int\limits_{S_d} v^{(2)} \lambda \left[(\mathbf{v}^{(1)} \cdot \mathbf{n})(\mathbf{d}^{(2)} \cdot \mathbf{e}^{(2)}) \right]$$

$$+ v^{(2)} \mu \left[\left(\mathbf{v}^{(1)} \cdot \mathbf{d}^{(2)} \right) \left(\mathbf{n} \cdot \mathbf{e}^{(2)} \right) + \left(\mathbf{v}^{(1)} \cdot \mathbf{e}^{(2)} \right) \left(\mathbf{n} \cdot \mathbf{d}^{(2)} \right) \right] \mathrm{d}S.$$

The scalar product $\mathbf{d}^{(2)} \cdot \mathbf{e}^{(2)}$ appearing in the above integral is identically equal to zero in the far field of receiving transducer, where the generated field approximates a semi plane wave. Accordingly, we can rewrite Eq. (4.20) in the shorter form:

$$(4.21) \quad F_B = \frac{1}{v_0^{(2)} V_{\text{T2}}} \int\limits_{S_d} v^{(2)} \mu \left[\left(\mathbf{v}^{(1)} \cdot \mathbf{d}^{(2)} \right) \left(\mathbf{n} \cdot \mathbf{e}^{(2)} \right) + \left(\mathbf{v}^{(1)} \cdot \mathbf{e}^{(2)} \right) \left(\mathbf{n} \cdot \mathbf{d}^{(2)} \right) \right] \mathrm{d}S.$$

Lame constant μ is given by the formula $\mu = \rho_2 V_{T2}^2$ and the product of $v^{(2)} \mathbf{d}^{(2)}$ is just equal the vector $\mathbf{v}^{(2)}$. Using this we can further transform Eq. (4.20) bringing it to the form:

$$(4.22) \quad F_B = \frac{z_2}{v_0^{(2)}} \int\limits_{S_d} \left[\left(\mathbf{v}^{(1)} \cdot \mathbf{v}^{(2)} \right) \left(\mathbf{n} \cdot \mathbf{e}^{(2)} \right) + \left(\mathbf{v}^{(1)} \cdot \mathbf{e}^{(2)} \right) \left(\mathbf{n} \cdot \mathbf{v}^{(2)} \right) \right] \mathrm{d}S.$$

All factors appearing in the Eq. (4.21) can be calculated from already derived formulas based on modified Rayleigh-Sommerfeld integral, Kirchhoff approximation and geometrical considerations. To this end we need parameters of transmitting and receiving transducer and position, size and orientation of the model defect implemented in the material.

Integral (4.22) provides a workable solution for numerical calculations of amplitudes of ultrasonic signals reflected from model defects of any size and orientation. It should be underlined that it has been derived using the Kirchhoff approximation and assumption that model defect is located in the far field of both transmitting and receiving transducer.

5. CONCLUSIONS

This article describes the theoretical model developed for computer simulation of ultrasonic testing of railway rails. The approach is based on well-established principles of elastodynamic theory such as Rayleigh-Sommerfeld integral, pencils model, Kirchhoff approximation, plane waves refraction and reflection formulas and reciprocity theorem. These major theoretical concepts were

put together to give workable solution for modelling of ultrasonic inspections of railway rails in real conditions. The approximations made in model development were carefully checked against the real testing circumstances. The relations between ultrasonic wavelength, tested object dimensions and defects sizes as well as the real nature of the sought defects (cracks) were taken into account in formulation of model assumptions and derivation of its main calculation formulas. Due to this the model is well adjusted to the practical reality of railway rails inspections.

The obtained solutions allow for computer simulation of several important aspects of ultrasonic inspection. First of all they enable effective calculation of ultrasonic fields generated in the rail material by typical ultrasonic probes used in non-destructive testing. This possibility is in itself very useful in planning of ultrasonic inspections but it is also a first step in calculation of ultrasonic echo amplitude obtained after interaction of ultrasonic wave with an internal defect. The possibility of calculation of amplitude of ultrasonic echo reflected from model defect of specified size and orientation positioned anywhere in the rail volume is the most important feature of the developed model. It enables computation of ultrasonic echo envelopes of specified model defects in the same form as it is done during practical ultrasonic inspections carried out with manual trolleys or inspection cars.

The derived formulas can be used in the modelling software being in preparation. The comparison of this software operation and the real measurements will enable formulation the final conclusions concerning the accuracy and limitations of developed theoretical model and practical usability of related inspection simulation software.

References

1. GRASSIE S.L., Rolling contact fatigue on the British railway system: treatment, *Wear*, **258**(7–8): 1310–1318, 2005, doi: 10.1016/j.wear.2004.03.065.

2. FRANKLIN F.J., KAPOOR A., Modelling wear and crack initiation in rails, *Proceedings of the Institution of Mechanical Engineers*, **221**(1): 23–33, 2007, doi: 10.1243/0954409JRRT60.

3. BOLTON P.J., CLAYTON P., Rolling-sliding wear damage in rail and tyre steels, *Wear*, **93**(2): 145–165, 1984, doi: 10.1016/0043-1648(84)90066-8.

4. CLAYTON P., ALLERY M.B.P., Metallurgical aspects of surface damage problems in rails, *Canadian Metallurgical Quarterly*, **21**(1): 31–46, 1982, doi: 10.1179/cmq.1982.21.1.31.

5. ZUMPANO G., MEO M., A new damage detection technique based on wave propagation for rails, *International Journal of Solids and Structures*, **43**(5): 1023–1046, 2006, doi: 10.1016/j.ijsolstr.2005.05.006.

6. Standard EN 16729-1, *Railway applications – Infrastructure – Non-destructive testing on rails in track – Part 1: Requirements for ultrasonic inspection and evaluation principles*, CEN, Brussels 2016.

7. Standard EN 16729-3, *Railway applications – Infrastructure – Non-destructive testing on rails in track – Part 3: Requirements for identifying internal and surface rail defects,* CEN, Brussels 2018.

8. Software Beam Tool 9, EclipseScientific 2020, https://www.eclipsescientific.com/software.html.

9. JOHNSON J.A., CARLSON N.M., TOW D.M., Ray trace calculations of ultrasonic fields, *Research in Nondestructive Evaluation*, **3**(1):27–39, 1991, doi: 10.1007/BF01606509.

10. BERGMANN A., ORTH T., KERSTING T., Ray tracing software for the layout of ultrasonic weld seam inspection, *e-Journal of Nondestructive Testing (NDT)*, **2**, 2009.

11. HARUMI K., UCHIDA M., Computer simulation of ultrasonics and its applications, *Journal of Nondestructive Evaluation*, **9**(2–3): 81–99, 1990.

12. Web site: http://www.onscale.com, 2021.

13. SCHMERR Jr. L.W., *Fundamentals of Ultrasonic Nondestructive Evaluation. A modelling approach*, 2nd ed., Springer AG Switzerland, 2016, doi: 10.1007/978-3-319-30463-2.

14. DESCHAMPS G.A., Ray techniques in electromagnetics, *Proceedings of the IEEE*, **60**(9): 1022–1035, 1972, doi: 10.1109/PROC.1972.8850.

15. CALMON P., LHÉMERY A., LECOEUR-TAÏBI I., RAILLON R., PARADIS L., Models for the computation of ultrasonic fields and their interaction with defects in realistic NDT configurations, *Nuclear Engineering and Design*, **180**(3): 271–283, 1998, doi: 10.1016/S0029-5493(97)00299-9.

16. RAILLON R., LECOEUR-TAÏBI I., Transient elastodynamic model for beam defect interaction: application to nondestructive testing, *Ultrasonics*, **38**(1–8): 527–530, 2000, doi: 10.1016/S0041-624X(99)00067-0.

17. GENGEMBRE N., Pencil method for ultrasonic beam computation, *5th World Congress on Ultrasonics*, Paris 2003.

18. AULD B.A., General electromechanical reciprocity relations applied to the calculation of elastic waves scattering coefficients, *Wave Motion*, **1**(1): 3–10, 1979, doi: 10.1016/0165-2125(79)90020-9.

19. SCHMERR Jr. L.W., Song S-J., *Ultrasonic Nondestructive Evaluation Systems. Models and Measurements*, Springer-Verlag US, 2007, doi: 10.1007/978-0-387-49063-2.

20. AULD B.A., *Acoustic Fields and Waves in Solids*, John Wiley & Sons, 1973.